J Mater Sci (2011) 46:7393–7400
DOI 10.1007/s10853-011-5700-8

Hydrogen peroxide versus water synthesis of bioglass–nanocrystalline hydroxyapatite composites

G. Melinte · L. Baia · V. Simon · S. Simon

Received: 21 July 2010 / Accepted: 15 November 2010 / Published online: 21 June 2011

Abstract This article reports a comparison of the structural and textural properties of bioglass–hydroxyapatite (HA) composites obtained in the SiO_2–CaO–P_2O_5 system by sol–gel method, with different amounts of hydrogen peroxide (3% H_2O_2) or water (H_2O). X-ray diffraction, Raman, and FT-IR spectroscopy reveal the presence of nanocrystalline HA. Scanning electron microscopy images illustrate that the HA phase is mainly distributed on the glass surface. The results point out that the sintering at 550 °C of a sol–gel derived SiO_2–CaO–P_2O_5 bioglass leads to a single crystalline phase of HA, and validate a new processing method for obtaining bioglass–HA composites. Structural analyses of the investigated composites indicate the existence of a silicate network built up from Q_3 and Q_2 units. The replacement of water with hydrogen peroxide has as consequence the increase of depolymerization degree of silica network. Textural properties were investigated with N_2-adsorption technique. The composites prepared with hydrogen peroxide exhibit a more uniform and narrow mesoporous distribution that recommends them for drug uptake and release applications. It was found that the specific surface area and pore volume are clearly influenced by the H_2O_2(H_2O):TEOS molar ratio.

Introduction

After 1969, when bioactive glasses were discovered [1], the strategy for bone tissue repair was to replace the bioinert materials of first-generation biomaterials with silica-based bioactive glasses of the second-generation biomaterials, which provided for the first time an alternative for interfacial bonding of an implant with host tissue [2]. The third-generation of biomaterials insures tissue regeneration using the gene activation properties of bioglass [3].

The bonding mechanisms of bioactive glasses to living tissue involve a sequence of 11 reactions steps. Steps 1–5 are chemical, steps 6–11 are related to the biological response [2]. Hench described the sequence of the first five stages that resulted in the formation of a hydroxy-carbonate apatite (HCA) layer on the surface of the bioactive glasses [4]. The first reaction is the ion exchange between the alkali in the glass and water. This is followed by a breakdown of the silica network, forming silanol bonds that repolymerize to form a hydrated, high surface-area, silica-rich layer. The silica-rich surface attracts organic molecules (proteins and collagen) and facilitates the formation of the HCA layer on the surface of the glass [5]. The HCA layer provides an ideal environment for the next six cellular reaction steps that include cells colonization followed by proliferation and differentiations of the cells to form a new bone that has a strong mechanical bond to the implant surface [6]. On the other hand, the behavior of bioactive glasses in the formation of new hard (bone) or soft (muscle) tissue is controlled by several factors, such as pore size distribution and porosity, interconnection of pores, specific surface area, bulk morphology and, obviously, glass composition [7].

Sol–gel derived bioglasses present several important advantages over those processed by standard melting and casting method. Sol–gel method enables the preparation of glasses at low synthesis temperature and expands the bioactive composition range up to 90 mol% SiO_2. It also allows to simplify the glass composition and particularly to

G. Melinte · L. Baia (✉) · V. Simon · S. Simon
Institute for Interdisciplinary Research in Bio-Nano-Sciences, Faculty of Physics, Babes-Bolyai University, M. Kogalniceanu 1, 400084 Cluj-Napoca, Romania
e-mail: lucian.baia@phys.ubbcluj.ro

avoid the addition of sodium oxide, used to reduce the melting temperature of the melt derived glasses. In addition, due to their higher purity, surface area and homogeneity, and to the presence of residual hydroxyl ions, sol–gel derived bioglasses exhibit higher bone bonding rates together with excellent degradation/bioresorption properties [6, 8, 9]. Furthermore, bioglasses prepared via sol–gel method always have an interconnected mesoporous structure, with pores about 5–10 nm in diameter [10]. The presence of hydroxyapatite (HA) offers beside several specific textural properties an important advantage concerning the bioactive character of the sol–gel derived bioglass–HA composites [11]. The superior bioactivity together with excellent mechanical properties and favorable microstructure made them suitable for obtaining scaffolds used in tissue engineering and regeneration [12, 13].

The purpose of this study was to determine the effect of $H_2O_2(H_2O)$:TEOS molar ratio on the textural and structural characteristics of the sol–gel-derived bioglass–HA composites obtained in the SiO_2–CaO–P_2O_5 system. Scanning electron microscopy (SEM), X-ray diffraction (XRD), vibrational spectroscopic techniques (Raman and FT-IR), and N_2-adsorption measurements have been used for this purpose.

Experimental

Sample preparation

The composition of the studied bioglasses is $60SiO_2$–$36CaO$–$4P_2O_5$ (mol %). They were prepared by sol–gel method as follows: tetraethyl orthosilicate (TEOS: $C_8H_{20}Si$) was mixed with absolute ethanol (C_2H_5-OH/Et-OH). The molar ratio Et-OH:TEOS was kept at 4:1. Different amounts of hydrogen peroxide (H_2O_2, 3%) or double distillate water were used to prepare calcium nitrate ($Ca(NO_3)_2{\cdot}4H_2O$) and dibasic ammonium phosphate ($(NH_4)_2HPO_4$) solutions. The $H_2O_2(H_2O)$:TEOS molar ratios together with the sample notation are presented in Table 1. Each solution was consecutively added to TEOS solution under continuous stirring. HCl (2 N) was added to catalyze the hydrolysis/condensation reactions. The final solutions were kept at room temperature until gelation occurs (4 days). The gels were aged for 10 days at room temperature and then they were sintered at 550 °C for 1/2 h.

Sample characterization

The XRD patterns were obtained with a Shimatzu XRD-6000 diffractometer, using CuKα radiation ($\lambda = 1.5418$ Å), with Ni-filter. The measurements were performed at a scan speed of 4° min^{-1} on a 2θ scan range of 10°–80° using for calibration quartz powder. Operating power of the X-ray source was 40 kV at 30 mA intensity.

The Raman spectra were recorded with a Witec confocal Raman system CRM 200 equipped with a X20/0.4 microscope objective and a 300 lines/mm grating. The 632.8 nm laser line with a power of 3 mW incident on the sample and a spectral resolution of about 7 cm^{-1} were employed.

The FT-IR spectra were obtained on a Bruker Equinox 55 spectrometer. The samples were powdered and mixed with KBr to obtain thin pellets with a thickness of about 0.3 mm. The spectral resolution was of 2 cm^{-1}.

The specific surface area, pore volume, and pore radius of the samples were obtained from N_2-adsorption measurements, using a Sorptomatic 1990 apparatus. The BET method was used for calculation of surface area, and the BJH method was used for determination of porosity parameters.

SEM images were recorded with a JEOL JSM 5510LV equipment.

Results

The X-ray diffractograms (Fig. 1) show the characteristics of a vitreous phase along with nanocrystalline HA. Five diffractions peaks are revealed at 25.7°, 31.78°, 32.19°,

Table 1 Textural and structural properties of the $60SiO_2$–$36CaO$–$4P_2O_5$ glass–ceramic bioglass–HA composites prepared with hydrogen peroxide and water

Sample molar ratio	H_2O_2:TEOS molar ratio	H_2O:TEOS molar ratio	BET surface area ($m^2\ g^{-1}$)	Pore volume ($cm^3\ g^{-1}$)	BJH modal pore diameter (nm)	BJH median pore diameter (nm)	A_2^Q/A_3^Q
A	15	–	65.3	0.186	8.60	8.61	0.27
B	10	–	103.1	0.267	7.45	7.68	0.2
C	5	–	75.7	0.211	7.97	8.19	0.52
A1	–	15	80.9	0.201	5.47	7.25	0.26
B1	–	10	88.9	0.255	6.90	8.51	0.44
C1	–	5	73.6	0.213	7.64	8.20	0.18

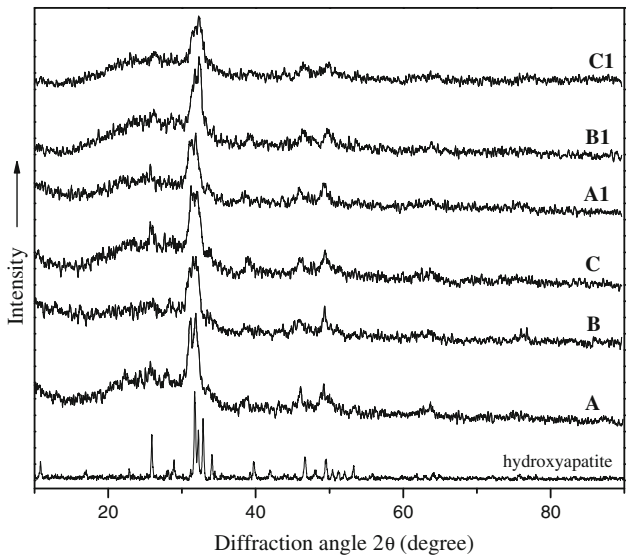

Fig. 1 XRD patterns of the $60SiO_2$–$36CaO$–$4P_2O_5$ bioglasses–HA composites prepared with hydrogen peroxide (*A*, *B*, and *C*), water (*A1*, *B1*, and *C1*) together with the standard diffractogram pattern for HA

38.8°, 46°, and 49.3° corresponding to the (002), (211), (112), (310), (222), and (213) reflection of HA phase [14, 15]. In order to clearly distinguish the HA phase, a standard pattern was inserted in Fig. 1 [16].

Composites morphology was evaluated by SEM. The recorded images of the samples B and B1 are illustrated in Fig. 2 and confirm the presence of HA crystals on the bioglass surface. The HA layer has about 3 μm thickness for both hydrogen peroxide and water-based samples and seems to be uniformly distributed on the relatively smooth surface of the glass matrix (Fig. 2a, b).

Nitrogen adsorption–desorption isotherms of the samples prepared with different amounts of water or hydrogen peroxide are shown in Fig. 3. An isotherm is the relationship, at constant temperature (77 K), between the amount of the adsorbed gas (usually expressed in $cm^3\ g^{-1}$) and the relative pressure p/p_0, where p_0 is the saturation pressure of pure nitrogen [17]. According to IUPAC classification, all obtained isotherms are of type IV, implying that each of these bioglass samples contain meso and micropores which are non-perfect cylindrical in shape. All the samples exhibit H1-type hysteresis loops, characterized by narrow steps and almost parallel adsorption and desorption branches. Such types of loops are given by adsorbents with a narrow distribution of uniform pores (e.g., open-ended tubular pores) [18].

Figure 4 illustrates the mesopores distribution as a function of the amount of hydrogen peroxide and water. The detailed data on specific surface area, pore volume, and pore size of each sample are summarized in Table 1. The H_2O-based samples exhibit a narrow mesopores size distribution with a modal pore diameter between 5 and 10 nm. The samples prepared with H_2O_2 give rise to a more uniform and narrow mesopores size distributions, with a modal pore diameter between 6.5 and 9 nm.

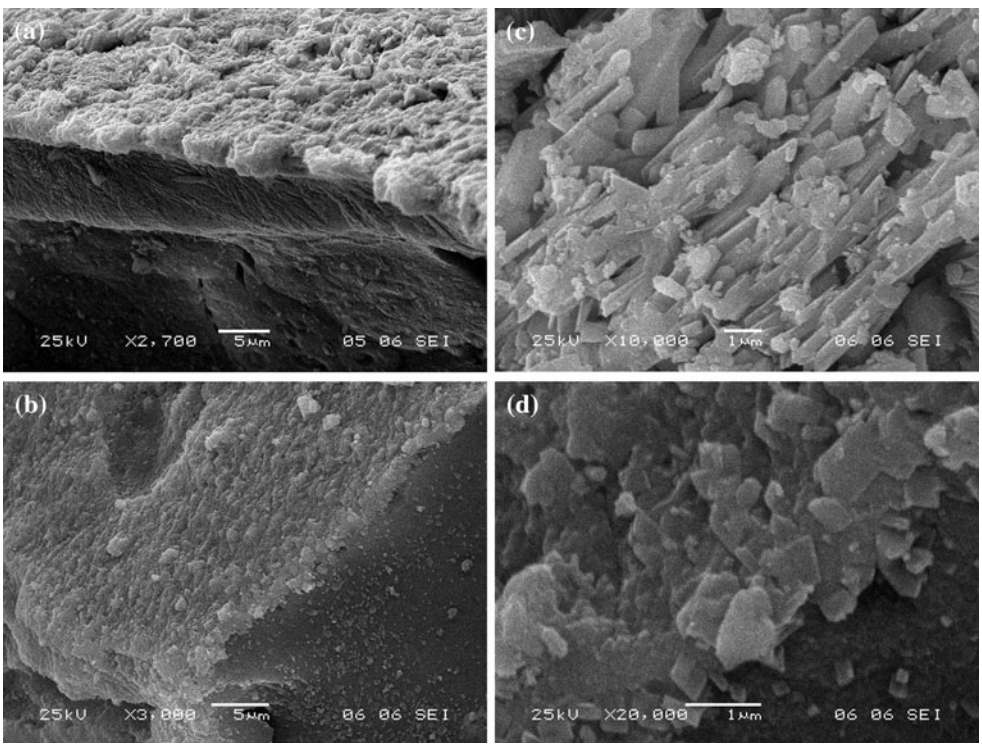

Fig. 2 SEM micrographs of the $60SiO_2$–$36CaO$–$4P_2O_5$ bioglass–HA composites prepared with hydrogen peroxide (**a** and **c**) and water (**b** and **d**)

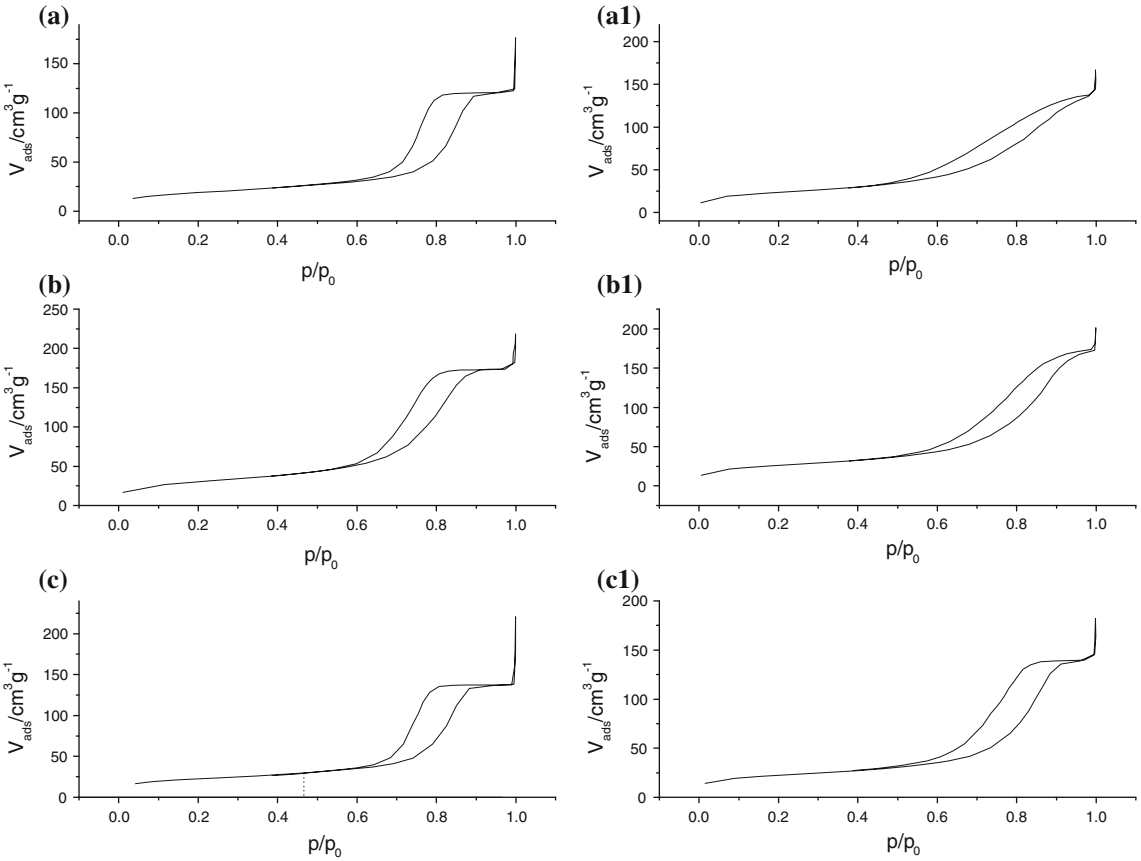

Fig. 3 Nitrogen adsorption–desorption isotherms of the $60SiO_2$–$36CaO$–$4P_2O_5$ bioglass–HA composites prepared with hydrogen peroxide (**a**, **b**, and **c**) and water (**a1**, **b1**, and **c1**)

The FT-IR spectra (Fig. 5) are dominated by a strong band between 850 and 1250 cm^{-1}. It is a combination of stretching vibrational modes of SiO_4 and PO_4 tetrahedra. The shoulder at 1225 cm^{-1} is assigned to the longitudinal optical Si–O–Si stretching mode [19]. The band situated at 1080 cm^{-1} is attributed to the stretching vibration of $Si–O^-$ bonds in the Q_3 tetrahedral units, while the shoulder at 950 cm^{-1} is due to the vibration of two non-bridging oxygen atoms in the Si–O–Si environment (Q_2 units) [20, 21]. The silanol vibrations signal (960 cm^{-1}) is superposed over the Q_2 units signal [22]. The band at about 1040 cm^{-1} is identified as P–O stretching vibrational mode of PO_4^{3-} tetrahedra from HA [9]. A strong band was also observed at 466 cm^{-1} and is considered to arise from the rocking motion of the bridging oxygen atoms perpendicularly to the Si–O–Si plane [19]. The band located around 800 cm^{-1} is assigned to the bending motion of oxygen atoms along the bisector of the Si–O–Si bridging group [19]. A doublet corresponding to P–O asymmetric bending vibrations in the PO_4 tetrahedra was observed at 569 and 605 cm^{-1} [23, 24]. The broad band between 3000 and 3700 cm^{-1} is assigned to stretching vibrations of O–H bonds [18, 25].

Raman spectroscopy is very sensitive to changes in the Si–O–Si environment of silica-based glasses and is a powerful technique used for the identification of tetrahedral units (Q_n). The Raman spectra of the $60SiO_2$–$36CaO$–$4P_2O_5$ bioglass–HA composites prepared with hydrogen peroxide and water reveal differences only in the spectral range between 850 and 1300 cm^{-1} (see Fig. 6). The stretching vibrations of silicon–single non-bridging oxygen atom in SiO_4 tetrahedra (Q_3 units) give rise to a strong band at 1092 cm^{-1} [26, 27]. The band between 1040 and 1080 cm^{-1} is attributed to the vibrations of $Si–O^0$ from bridging oxygen atoms in structural units that contain non-bridging oxygens (both Q_2 and Q_3 units) [28]. A week signal assigned to the internal modes of PO_4^{3-} units appears around 1025 cm^{-1} [29]. The Raman spectra also exhibit a strong band at 966 cm^{-1} that is due to the superposition of $Si–O^-$ stretching vibrations in silicate tetrahedral units with two non-bridging oxygen atoms

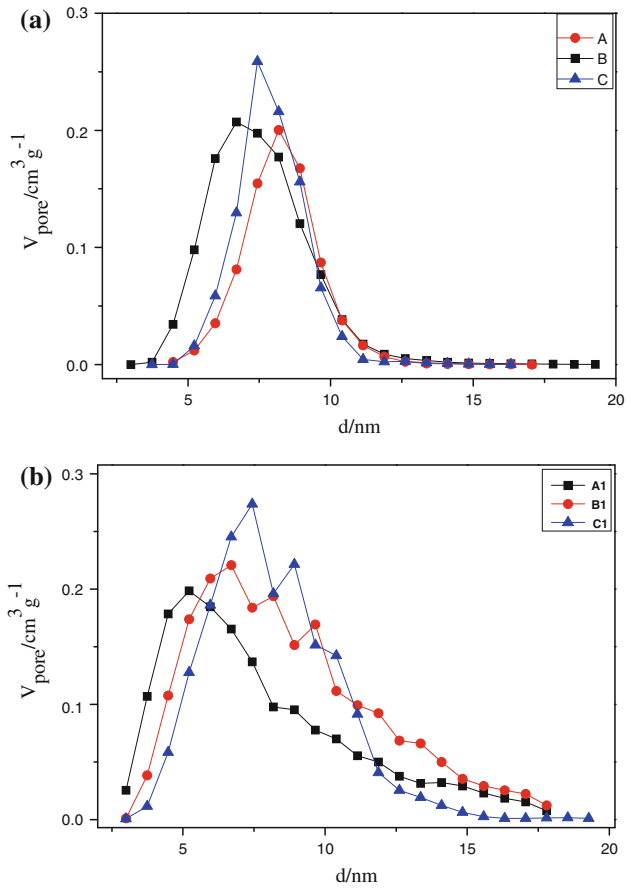

Fig. 4 Textural pore size distribution of the $60SiO_2$–$36CaO$–$4P_2O_5$ bioglass–HA composites prepared with hydrogen peroxide (**a**) and water (**b**), obtained from BJH analysis of nitrogen desorption branch

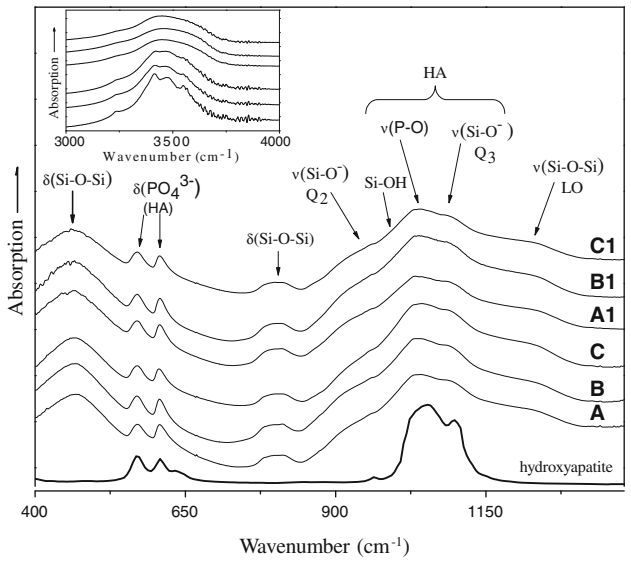

Fig. 5 FT-IR spectra of the $60SiO_2$–$36CaO$–$4P_2O_5$ bioglass–HA composites prepared with hydrogen peroxide (*A*, *B*, and *C*), water (*A1*, *B1*, and *C1*) together with the standard FT-IR spectrum of HA. The *inset* shows the spectral domain between 3000 and 3700 cm^{-1}

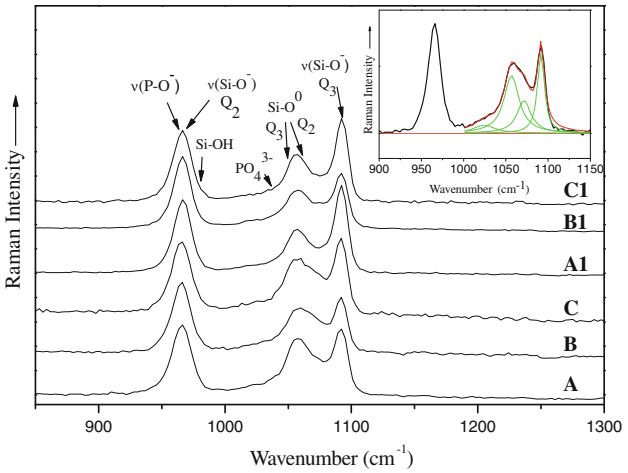

Fig. 6 Raman spectra of the $60SiO_2$–$36CaO$–$4P_2O_5$ bioglass–HA composites prepared with hydrogen peroxide (*A*, *B*, and *C*) and water (*A1*, *B1*, and *C1*). The *inset* shows the deconvoluted spectral range between 1000 and 1150 cm^{-1}

(Q_2 units) with the P–O$^-$ stretching vibrations of PO_4 tetrahedra. It should be emphasized that silanol vibrations (980 cm^{-1}) also contribute to the appearance of this band [19, 21, 26].

Discussion

The crystalline HA phase developed in $60SiO_2$–$36CaO$–$4P_2O_5$ sol–gel derived samples after the heat treatment at 550 °C (Fig. 1) consists of crystallites with the size of 8.8 nm, as determined using Scherrer equation applied to the peak located at 25.7°. The crystallites size (~54 nm) of standard HA gives rise, as expected, to more narrow diffraction peaks relative to those of HA from the investigated composites.

It is important to emphasize the relative low temperature (550 °C), where the conversion of calcium-phospho-silicate glass with low phosphorus content into a glass–ceramic sample takes place. Very recently Ravarian et al. [30] reported on sol–gel synthesis and properties of $64SiO_2$–$31CaO$–$5P_2O_5$ (mol %) bioglasses prepared with TEOS, triethyl phosphate, and calcium nitrate in water solutions. After heating at 700 °C for 24 h, the bioglass is approximately amorphous, with germs of pseudowollastonite and alpha-tricalcium phosphate, and only after heating at 1000 °C for 3 h the bioglass was converted into a glass–ceramic with pseudowollastonite and alpha-tricalcium phosphate crystalline phases. This bioglass was further used to prepare composite samples by mixing with HA and heating at different temperatures up to 1000 °C that is much higher than the temperature of 550 °C, at which we obtained the bioglass–HA composites.

The presence of nanocrystalline HA by XRD is confirmed by the SEM micrographs (Fig. 2) that show the HA layer formed on the bioglass surface. The shape of HA crystals seems to be affected by the presence of hydrogen peroxide that leads to needle-like crystals with lengths about 3–5 μm (Fig. 2c), while for the water-based samples the HA crystals show a rough shape (Fig. 2d).

Depending on the synthesis conditions of $60SiO_2$–$36CaO$–$4P_2O_5$ sol–gel derived samples, using water or hydrogen peroxide, the textural properties are changed. The major difference between adsorption isotherms of bioglass samples takes place at the p/p_0 value where the capillary condensation appears. This difference is in a direct relation with the average pores size: the smaller the pores, the lower pressure is required for the capillary condensation [31]. The shift of the onset of capillary condensation towards lower or higher relative pressure as shown in Fig. 3 is in agreement with the median pores radius displayed in Table 1. On the other hand, the width of the hysteresis is an indicative of the pores interconnectivity: the wider the hysteresis, the more interconnected are the pores [32]. By comparing the hysteresis widths obtained for water-based samples B1 and C1 with those obtained from the bioglasses prepared with hydrogen peroxide, samples B and C, one observes a slight increase of pores interconnectivity for the latter pairs of samples. A more considerably difference can be seen between the hystereses recorded for samples A and A1, where a substantial improvement of pores interconnectivity is observed for hydrogen per oxide-based sample. An interconnected mesopores network provides better nutrient delivery, bone ingrowths, and eventually vascularization; therefore, it allows a better in vivo bioactivity [33].

For both type of samples, the specific surface area and the pore volume reach the highest value for the medium water or hydrogen peroxide content (Table 1). According to the literature, the high specific area is beneficial for tissue engineering applications because it can accelerate surface crystallization of HA, promote the degradation rate, and aid attachment and migration of cells inside the scaffold [34, 35]. In vitro studies showed the improvement of dissolution rate in silica gel-glass as pore volume increased [2].

Uniform and narrow pore size distribution is obtained for the samples prepared with hydrogen peroxide (Fig. 4a). Usually, this type of pore size distribution centered on 7 nm indicates a well-ordered structure [36]. It was found that silica glasses with a highly ordered mesoporous structure have superior bioactivity properties and also a remarkable capability of controlled drug delivery [35, 37].

The FT-IR spectra (Fig. 5) indicate the presence of crystalline HA (bands at 569, 605, and 1040 cm^{-1} attributed to PO_4 unit vibrations). The FT-IR spectrum of pure HA exhibits a very intense and broad band, occurring from three absorption peaks, between 900 and 1200 cm^{-1} with the highest intensity reached around 1040 cm^{-1} [38]. The presence of these spectral features can be easily followed by simply comparing the IR spectrum of the standard HA, which is inserted in Fig. 5, with those of the investigated composites. Due to the overlapping of the tetrahedral SiO_4 unit vibrations with the main bands of the crystalline HA, it is very difficult to identify the spectral changes associated with the structural modification of SiO_4 tetrahedra. No major differences between the spectra of the H_2O_2 and H_2O samples occur in the spectral range between 400 and 4000 cm^{-1}, excepting a slight increase in intensity of the bands, from the spectra recorded on samples prepared with hydrogen peroxide, located between 3000 and 3700 cm^{-1} that were attributed to vibrations of silanol groups and adsorbed molecular water (see the inset from Fig. 5) [18, 25]. Moreover, the intensity of this band is enhanced with the increasing of hydrogen peroxide amount. It was reported that the silanol groups found in the mesopore walls have the ability to adsorb molecules of pharmacological interest [39]. That means that the bioglasses prepared with hydrogen peroxide could be successfully used for enhancing drug delivery capabilities.

Raman spectroscopy was further employed for identifying the structural differences between water and hydrogen peroxide-based bioglasses (see Fig. 6). For analyzing the depolymerization degree of the silica network, it is necessary to know the value of the ratio between the areas of the bands assigned to Q_2 and Q_3 unit vibrations (A^{Q2}/A^{Q3}). Since the bands given by Q_2 unit vibrations are overlapped with those of HA, which appear in the spectral domain between 940 and 980 cm^{-1}, the assessment of the above mentioned areas ratio becomes extremely difficult for this spectral range. As can be observed in the Raman spectra, the band between 1030 and 1080 cm^{-1} shows a pronounced asymmetry to the right (a shoulder broadens the band) for hydrogen peroxide-based samples. This band is made up from convoluted signals given by $Si–O^0$ vibrations in both Q_2 and Q_3 tetrahedral units. The contribution of Q_2 units can be observed at higher wavenumbers, while that of Q_3 units give rise to a signal at lower wavenumber values (Fig. 6). The asymmetry of this band originates from the variation in relative intensities of Q_2 and Q_3 bands. Consequently, the deconvolution of the spectral domain between 1000 and 1150 cm^{-1} becomes necessary due to the additional contribution of both phosphate and Q_3 units from ca. 1020 and 1080 cm^{-1}, respectively. For all the samples, the band attributed to the Q_2 units is located at about 1075 cm^{-1}, while the Q_3 units band appears at 1057 cm^{-1}. The ratio between the areas of these bands (A^{Q2}/A^{Q3}) is shown in the Table 1. As can be observed the highest values of areas ratio A^{Q2}/A^{Q3} are obtained for the hydrogen peroxide-based samples. The

most significant difference appears between the samples pairs B and B1 and C and C1. For B1 sample, the A^{Q2}/A^{Q3} area ratio is about two times higher than for B sample prepared with hydrogen peroxide, while for C sample it is about three times higher than for C1 sample. This behavior can be easily associated with a decrease in number of Q_3 groups and/or an increase of Q_2 groups number and reveals the increasing of the depolymerization degree of the silica network for hydrogen peroxide samples, mainly for samples B and C. In spite of the network fragmentation, when the hydrogen peroxide is used, the number of Q_3 units remains high and no other Q_0 and Q_1 units are formed. Taking into consideration that an improved bioactivity is closely related to an increase of the number of Q_2 and Q_3 units [19, 26, 40, 41] and having in view the obvious morphological improvements observed for the samples prepared with H_2O_2 in comparison with water-based bioglasses one can expect a better bioactivity for hydrogen per oxide-based samples.

Conclusions

Bioglass–HA composites have been prepared by sol–gel method with different amounts of hydrogen peroxide or water. The heat treatment applied to the samples at 550 °C for 30 min induced the development of a nanocrystalline HA structure that has been found to be mainly dispersed on the bioglass surface.

Raman spectroscopy showed that the silicate network of the bioglasses is built up from Q_3 and Q_2 units. The hydrogen peroxide-based samples exhibit an increase of the depolymerization degree of the silica network in comparison with water-based bioglasses, mostly for the samples with middle and lower concentration, that structure becomes less connected. The HA signature was evidenced for all investigated samples. The hydrogen per oxide-based bioglasses exhibit a more uniform and narrow mesoporous distribution and a better pores interconnectivity. Moreover, the maximum value of specific surface area and pore volume was obtained for the sample with a molar ratio H_2O_2:TEOS of 10:1. The shape of HA crystals determined by SEM images was found to be needle-like crystals with lengths of about 3–5 μm for hydrogen per oxide-based samples, while for the water-based samples the crystals show a rough shape. The developed HA layer was determined to be of about 3 μm thickness for both hydrogen peroxide and water-based samples.

Acknowledgements This research was accomplished in the framework of PNII PCCE-101/2008 project granted by the Romanian National University Research Council—CNCSIS.

References

1. Hench LL (2006) J Mater Sci Mater Med 17:967
2. Hench LL, Jones JR, Sepulveda P (2002) In: Polak JM, Hench LL, Kemp P (eds) Bioactive materials for tissue engineering scaffolds. Imperial College Press, London
3. Hench LL, Polak JM (2002) Science 295:1014
4. Hench LL, Splinter RJ, Allen WC, Greenlee TK (1971) J Biomed Mater Res 2:117
5. Froum SJ, Weinberg MA, Tarnow D (1998) J Periodontol 69(6): 698
6. Zhong JP, Greenspan DGJ (2000) Biomed Mater Res 53:694
7. Tilocca A, Cormack AN (2010) Langmuir 26(1):545
8. Hamadouche M, Meunier A, Greenspan DC, Blanchat C, Zhong JP, LaTorre GP (2001) J Biomed Mater Res 54:560
9. Mami M, Lucas-Girot A, Oudadesse H, Srid RD, Mezahi F, Dietrich E (2008) Appl Surf Sci 254:7386
10. Li N, Je Q, Zhu S, Wang R (2005) Ceram Int 31:641
11. Diaz A, Lopez T, Manjarrez J, Basaldella E, Martinez-Blanes JM, Odriozola JA (2006) Acta Biomater 2:173
12. Yunos DM, Bretcanu O, Boccaccini AR (2008) J Mater Sci 43:4433. doi:10.1007/s10853-008-2552-y
13. Novak S, Druce J, Chen QZ, Boccaccini AR (2009) J Mater Sci 44:1442. doi:10.1007/s10853-008-2858-9
14. Balamurugan A, Sockalingum G, Michel J, Faure J, Banchet V, Wortham L, Bouthors S, Laurent-Maquin D, Balossier G (2006) Mater Lett 60:3752
15. Lei B, Chen X, Wang Y, Zhao N, Du C, Fang L (2009) J Non-Cryst Solids 355:2678
16. Downs RT (2006) Database for minerals. http://rruff.info. Accessed 12 Oct 2010
17. Jones JR, Ehrenfried LM, Hench LL (2006) Biomaterials 27:964
18. Rouquerol F, Rouquerol J, Sing K (1999) Adsorption by powders & porous solids. Academic Press, San Diego
19. Chrissanthopoulos A, Bouropoulos AN, Yannopoulos SN (2008) Vib Spectrosc 48:118
20. Domine F, Piriou B (1983) J Non-Cryst Solids 55:125
21. Pryce RS, Hench LL (2004) J Mater Chem 14:2303
22. Stolen RH, Walnfen GE (1976) J Chem Phys 64:2623
23. Pereira MM, Clark AE, Hench LL (1995) J Am Ceram Soc 78(9):2463
24. Laczka M, Cholewa-Kowalska K, Laczka-Osyczka A, Tworzydlo M, Turyna B (2000) J Biomed Mater Res 52:601
25. Smith B (1999) Infrared spectra interpretation: a systematic approach. CRC Press, Boca Raton
26. Agathopoulosa S, Tulyaganova DU, Venturaa JMG, Kannana S, Karakassidesc MA, Ferreiraa JMF (2006) Biomaterials 27:1832
27. Furukawa T, White WB (1980) J Non-Cryst Solids 38(39):87
28. Lasaga AC (1982) Phys Chem Miner 8:36
29. de Aza PN, Guitian F, Santos C, de Aza S, Cusco R, Artus L (1997) Chem Mater 9:916
30. Ravarian R, Moztarzadeh F, Solati HM, Rabiee SM, Khoshakhlagh P, Tahriri M (2010) Ceram Int 36:291
31. Krawiec P (2006) Nanostructured porous high surface area ceramics for catalytic applications. PhD Thesis, Dresden
32. Colomer MT (2006) Adv Mater 18:371
33. Huang LF, Lu PS, Chiou LC, Chang IL, Shih CJ (2009) IFMBE Proceedings. doi:10.1007/978-3-540-92841-6_337
34. Peltola T, Jokinen M, Rahiala H, Levanen E, Rosenholm J, Kangasniemi I, Yli-Urpo A (1999) J Biomed Mater Res 44:2
35. Izqyuedo-Barba I, Colilla M, Vallet-Regi M (2008) J Nanomater 3:1
36. Souza KC, Ardisson JD, Sousa EM (2009) J Mater Sci Mater Med 20:507

37. Yan X, Huang X, Yu C, Deng H, Wang Y, Zhang Z, Qiao S, Lu G, Zhao D (2006) Biomaterials 27(18):3396
38. National Institute of Standard and Tehnology (2010) http://webbook.nist.gov. Accessed 12 Oct 2010
39. Ramida A, Munoz B, Pariente JP, Vallet-Regi M (2003) J Sol-Gel Sci Technol 26:1199
40. Serra J, Gonzalez P, Liste S, Chiussi S, Leon B, Perez-Amor M, Ylanen HO, Hupa M (2002) J Mater Sci Mater Med 13:1221
41. Aguiar H, Solla EL, Serra J, González P, León B, Almeida N, Cachinho S, Davim EJC, Correia R, Oliveira JM, Fernandes MHV (2008) J Non-Cryst Solids 354:4075